ACS Catalysis

Research Article

pubs.acs.org/acscatalysis

Bifunctional Tandem Catalysis on Multilamellar Organic–Inorganic Hybrid Zeolites

Le Xu, Chen-geng Li, Kun Zhang, and Peng Wu*

Shanghai Key Laboratory of Green Chemistry and Chemical Processes, Department of Chemistry, East China Normal University, North Zhongshan Road 3663, Shanghai 200062, P. R. China

Supporting Information

ABSTRACT: Tandem catalysis has been realized on the multilayered zeolites with organic-structure-directing agent (OSDA) molecules occluded within micropores. A combination of mild acid treatment and ion-exchange with ammonia solution was carried out on as-synthesized multilamellar MFI aluminosilicate, giving rise to an acid–base bifunctional catalyst. Containing tripropyl head groups, the Gemini-type quaternary ammonium OSDAs were firmly immobilized in the intersection of straight and sinusoidal 10-membered ring channels, with the other one exposed to the layer surface of the nanosheets. The resulting organic–inorganic materials possessed simultaneously the acid sites related to the framework Al and the base sites derived from coexisting OSDAs. In particular, two types of base sites were present, that is, the Lewis base sites due to the SiO^- species and Brønsted base sites due to the OH^- counteranion of exposed quaternary ammonium cations. The rigid materials were highly active and reusable in the one-pot reaction of tandem deacetalization–Knoevenagel condensation. Supporting palladium nanoparticles (Pd NPs) on the organic–inorganic hybrid zeolite led to bifunctional catalysts, which catalyzed effectively one-pot synthesis of benzylidene malononitrile from benzyl alcohol under soluble-base-free conditions, in which the benzyl alcohol was first aerobic oxidized to intermediate benzaldehyde followed by Knoevenagel condensation with malononitrile.

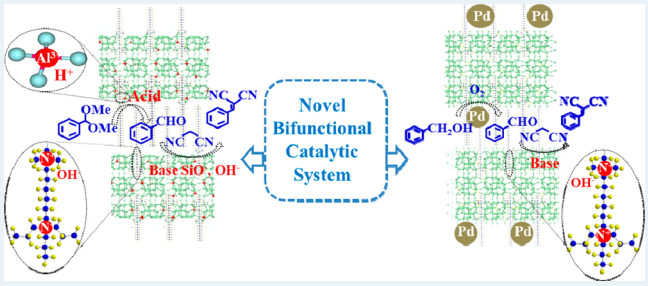

KEYWORDS: *bifunctional catalysis, hybrid material, multilamellar, tandem reaction, zeolites*

1. INTRODUCTION

Zeolites are widely used in catalysis, adsorption, and separation processes, because of well-defined crystalline structures, unique channel systems of molecular dimension, changeable chemical compositions, as well as controllable morphology.[1] Generally, high silica zeolites require using organic amines or ammonium cations in hydrothermal synthesis. The roles of amines or quaternary ammoniums in the construction of zeolite structures are categorized into three categories, for example, pore space-filler, template, and organic-structure-directing agent (OSDA).[2] In recent years, many efforts have been devoted to synthesize new zeolites through the strategy of designing novel OSDA molecules. Thus, a number of zeolites with novel crystalline structures have been developed, including SSZ,[3] ITQ,[4] and TNU series.[5]

Playing important roles in the steps of nucleation and crystal growth, the mission of OSDA, however, is almost accomplished when a full crystallization of zeolites is realized. Thus, almost without exception, the occluded organic species are burned off to make the zeolite micropores open and accessible. The removal of expensive OSDA not only leads to waste disposal but also increases the manufacture cost of materials. Thus, it is of great research interest to explore the potential utilization values of the used OSDAs. Davis et al. once developed a combustion-free methodology for ZSM-5 synthesis by recycling those occluded OSDA species. The OSDA synthesized by bimolecular condensation was disassembled to two parts of smaller fragments that could be extracted out of the zeolite channels, and these fragments were then reassembled and reused successfully as OSDA in the second synthesis.[6] In addition to this kind of recycle process, researchers have been looking for other effective methods to take advantage of OSDAs occluded in zeolite channels, especially from the catalytic point of view. Kubota et al. once employed the as-synthesized Beta zeolite containing tetraethylammonium (TEA^+) cations to catalyze the Knoevenagel condensation. The hybrid Beta zeolite proved to be a good base catalyst under mild conditions and the SiO^- moieties located at the pore-mouth, that were assisted by coexisted TEA^+ cations, were presumed to be the active sites.[7] However, the TEA^+ cations with a relatively small size were extracted readily out of the 12-membered ring (MR) channels of beta zeolites by acid treatment,[8] which would cause leaching problem in organic reactions.

It is commonly accepted that the organic species immobilized in mesoporous silica materials, such as MCM-41

Received: May 12, 2014
Revised: July 22, 2014
Published: July 23, 2014

   dx.doi.org/10.1021/cs500653p | ACS Catal. 2014, 4, 2959–2968

and SBA-15, either by direct synthesis or postgrafting, serve as efficient catalytic active sites, because the mesopores with large dimensions are accessible to guest molecules.[9] In this sense, the design synthesis of organic−inorganic heterogeneous acid, base or acid/base bifunctional catalysts have been realized successfully on the basis of mesoporous silica via a complicated functionalization procedure. In this study, we envision whether the OSDA species in microporous zeolites could be directly utilized as catalytic active sites rather than nonproductive decomposition by calcination. To serve as stable and reusable active sites in heterogeneous catalysis, the OSDA species should be firmly locked inside zeolite channels, but they also need to be reachable by reactant molecules. However, the OSDA species occluded in conventional zeolites are generally hardly accessible to reactants. For example, the quaternary ammoniums from tetrapropylammonium hydroxide (TPAOH), a common OSDA for MFI zeolites, are located at the intersections of straight 10-MR channels and sinusoidal 10-MR channels. Although the TPA^+ cations are stable against leaching, they are inaccessible to the molecules outside of the pores. Therefore, novel zeolite materials with specific structures fundamentally different from conventional ones are highly demanded.

Recently, a multilamellar zeolite consisting of the MFI nanosheets was synthesized by using various bifunctional Gemini-type OSDAs.[10] The quaternary diammonium head groups of this kind of OSDA play an important role in the crystallization of MFI nanosheets, whereas the long alkyl groups suppress regular crystal growth and stacking of the MFI nanosheets, giving rise to interlayer structures composed of nanosheets in unit cell scale. Removing the surfactant by calcination caused a partial condensation between the MFI layer and then leading to the mesopore-containing MFI zeolites. This facilitated the reactants with large molecular dimension to access the active sites in catalytic reactions. Thus, the calcined aluminosilicate and titanosilicate nanosheets with the MFI structure exhibited a catalytic performance superior to conventional bulk zeolites in a variety of reactions.[11] Considering the fact that these bifunctional OSDAs are difficult to synthesize and expensive in manufacturing cost, it would be preferable to increase their utilization values after finishing up zeolite crystallization rather than simple combustion.

Herein, we disclose a strategy to utilize OSDAs in as-synthesized multilamellar MFI zeolites for catalytic applications for the first time. The nanosheets firmly immobilize one quaternary ammonium group of well-chosen Gemini-type OSDAs, with half of the ammonium groups reachable from outside. The coexistence of OSDAs endows the multilamellar zeolites base sites, leading to a bifunctional catalyst useful for tandem deacetalization−Knoevenagel condensation with the combination of the framework Al-related acid sites. On the other hand, supporting palladium NPs onto organic−inorganic multilamellar MFI silicalite results in a bifunctional material that catalyzes effectively the one-pot synthesis of benzylidene malononitrile from benzyl alcohol in the absence of soluble base.

2. EXPERIMENTAL SECTION

2.1. Synthesis of Organic-Structure-Directing Agent. The OSDAs were synthesized following the procedures reported previously.[10] First, $[C_{18}H_{37}Me_2N^+(CH_2)_6Br]Br^-$, $C_{18-6-Br}$, was synthesized by a reaction of 0.01 mol of *N,N*-dimethyloctadecylamine (85%, TCI) with 0.1 mol of 1,6-dibromohexane (98%, Aladdin) in an acetonitrile/toluene mixture (300 mL, 1:1 v/v). The mixture was heated at 343 K for 12 h under stirring. After evaporating the solvents, the $C_{18-6-Br}$ solid was filtered and purified. Second, 0.01 mol of $C_{18-6-Br}$ was mixed with 0.02 mol of tripropylamine (98%, TCI) in chloroform (50 mL) and stirred under refluxing condition for 12 h. After solvent evaporation, the solid product of $[C_{18}H_{37}Me_2N^+(CH_2)_6N^+(Pr_3)]Br_2^-$ was obtained (denoted as OSDA-Pr). Similarly, $[C_{22}H_{45}Me_2N^+(CH_2)_6N^+Me_2C_6H_{13}]Br_2^-$ (denoted as OSDA-Me) was synthesized following the literature.[10a,b]

2.2. Zeolite Synthesis. The OSDA-Pr in bromide form was used for the hydrothermal synthesis of multilamellar MFI zeolites (LZSM-5 for aluminosilicate, LS for silicalite). The synthesis procedures were according to the literature but with a slight modification.[10] In a typical synthesis, OSDA-Pr, NaOH, $Al_2(SO_4)_3{\cdot}18H_2O$, H_2SO_4, and H_2O were mixed to obtain a clear aqueous solution, into which a desirable amount of TEOS was added dropwise. EtOH from the hydrolysis of TEOS was evaporated at 333 K for 2 h, leading to a gel composition of 100 SiO_2/0−0.72 Al_2O_3/10 OSDA/60 NaOH/18 H_2SO_4/4000 H_2O. The resultant homogeneous gel was transferred into a Teflon-lined stainless steel autoclave and heated at 423 K for 5 days. The product was filtered, washed with distilled water, and dried at 353 K overnight. The as-synthesized zeolite thus obtained was denoted as LZSM-5-as or LS-as.

For control experiments, OSDA-Me was also employed as OSDA to synthesize multilamellar ZSM-5 (denoted as LZSM-5-Me-as).[10a] ZSM-5 (Si/Al = 65) and silicalite-1 (S-1) with a bulk crystal morphology was synthesized by using TPA^+ as OSDA according to the conventional method reported previously.[12]

2.3. Preparation of Acid−Base Bifunctional Catalyst. To remove physically adsorbed OSDA-Pr species and recover the acid site located on the external surface of zeolite layers, the as-made sample was extracted in 1 mol L^{-1} HCl/EtOH solution at 333 K for 3 h at a solid-to-liquid weight ratio of 1:30. The resultant sample was denoted as LZSM-5-AT. To check the stability of remaining OSDA-Pr, the acid treatment was repeated. The acid treated samples were further stirred in 0.2 M aqueous ammonia solution for 1 h to ion-exchange counteranion with OH^-. The product was collected by filtration and rinsed with deionized water, giving rise to LZSM-5-AT−OH^- catalyst. For comparison, acid treatments were carried out on LZSM-5-Me-as, resulting in corresponding LZSM-5-Me-AT and LZSM-5-Me-AT2, respectively.

2.4. Loading Pd NPs onto Pure Silica Multilamellar MFI Nanosheets. Prior to supporting Pd NPs, a mild acid treatment and an ion-exchange with ammonia solution were carried out on LS-as according to aforementioned procedure. Then, 0.5 g of LS-AT−OH^- was added into 3 mL of toluene solution containing 0.005 g $Pd(OAc)_2$. After stirring for 2 h at room temperature, the solid was separated by centrifugation, washed with toluene, and dried in vacuum. The resultant LS-AT−OH^- coordinated with Pd^{2+} species was reduced with $NaBH_4$ in a solution of toluene and ethanol (v/v = 20:1). After separation by centrifugation and drying in vacuum, the Pd/LS-AT−OH^- sample was obtained. In control experiments, Pd NPs were loaded on S-1 and LS-AT-cal according to the same procedures.

2.5. Catalytic Reactions. The Knoevenagel condensation reaction of benzaldehyde with malononitrile was carried out at 353 K in toluene under N_2 for 1 h. In a typical run, the catalyst (50 mg), benzaldehyde (2 mmol), malononitrile (2 mmol), and toluene (3.6 g) were mixed in a flask connected to a cooling condenser. Then the flask was immersed in a water bath equipped with a magnetic stirrer. The products were separated by filtration and analyzed on a gas chromatograph (GC).

The one-pot tandem deacetalization−Knoevenagel condensation reaction was carried out by placing the catalyst (50 mg), benzaldehyde diemethylacetal (5 mmol), malononitrile (5 mmol), acetonitrile (2 mL), and H_2O (20 μg) in a glass flask. The resulting mixture was vigorously stirred at 353 K for a desired time under N_2. The products were separated by filtration and analyzed on GC.

The one-pot tandem aerobic oxidation−Knoevenagel condensation reaction was carried out in a glass flask equipped with a condenser. In a typical run, alcohol (2 mmol), Pd catalyst (200 mg), *n*-dodecane (0.1

dx.doi.org/10.1021/cs500653p | ACS Catal. 2014, 4, 2959−2968

mmol, internal standard), and toluene (10 mL) were heated at 358 K, during which they were charged into the reaction mixture at flow rate of 20 mL min^{-1}. After the reaction for a desired period of time, the oxygen flow was stopped, and then methylene compounds (2 mmol), such as malononitrile, ethyl cyanoacetate, or diethyl malonate, were charged into the mixture rapidly. The mixture was left at 358 K for another period of time. After the products were cooled and the solid catalyst was removed by centrifugation, the reaction products were analyzed by GC and GC-MS.

2.6. Characterization Methods. The X-ray diffraction (XRD) patterns were collected on a Rigaku Ultima IV X-ray diffractometer using Cu Kα radiation (λ = 1.5405 Å) at 35 kV and 30 mA. The nitrogen adsorption isotherms were recorded at 77 K on a BELSORP-MAX instrument after activating the samples at 393 K under vacuum at least for 5 h. The pretreatment temperature of 393 K was chosen in order to avoid thermal decomposition of OSDA. The specific surface area was evaluated using the Brunauer–Emmett–Teller (BET) equation and the total pore volume was calculated from the nitrogen adsorption amount at P/P_0 of 0.95. The pore size distribution was calculated for mesopores from the desorption isotherm using Barrett–Joyner–Halenda (BJH) method. The SEM images were taken on a Hitachi S-4800 microscope, whereas the TEM images were taken on a JEOL-JEM-2100 microscope. The amounts of Si, Al were quantified by inductively coupled plasma (ICP) on a Thermo IRIS Intrepid II XSP atomic emission spectrometer, whereas the C and N contents were determined with an ElementarVario EL III analyzer. The thermogravimetric and differential thermal analyses (TG-DTA) were performed on a METTLER TOLEDO TGA/SDTA851^e apparatus from 298 to 1073 K at a heating rate of 10 K min^{-1} in air. Solid-state NMR spectra were recorded on a VARIAN VNMRS-400WB NMR spectrometer. Fourier transform infrared (FT-IR) spectra were collected on a Thermo Scientific Nicolet Fourier transform infrared spectrometer (iS10). The analysis of organic phases were performed on a gas chromatography (Shimadzu 2014, FID detector) equipped with a 30 m OV-1 capillary column and a GC-MS (Agilent 6890 series GC system, 5937 network mass selective detector).

3. RESULTS AND DISCUSSION

3.1. Synthesis of Multilamellar Organic–Inorganic Hybrid LZSM-5 Zeolites. Multilamellar MFI nanosheets have been successfully synthesized by using various surfactants as OSDAs.[10,13] Among them, the most representative surfactant used is $C_{22}H_{45}Me_2N^+(CH_2)_6N^+Me_2C_6H_{13}]Br_2^-$, denoted as OSDA-Me, which was composed of two quaternary ammonium groups spaced by a C_6 alkyl group as well as a long-chain alkyl group (Scheme S1a).[10a,b] The diammonium group of the surfactant played the structure-directing role in the formation of MFI unit cells, and one of the diammonium groups was thus presumed to be located at the intersection of two 10-MR channels. Moreover, the long-chain alkyl group with hydrophobic characteristic restricted the crystal growth along *b*-axis, resulting in an ordered multilamellar organic–inorganic hybrid zeolite.[10] Removal of the surfactant by calcination caused a partial condensation between the MFI layers, leading to the MFI zeolite nanosheets with unit cell thickness.

In this study, we chose $[C_{18}H_{37}Me_2N^+(CH_2)_6N^+(Pr_3)]Br_2^-$ surfactant ($C_{18-6-3}Br_2$, named as OSDA-Pr, Scheme S1b) as OSDA to direct the multilamellar MFI nanosheets (LZSM-5-as). It should be noted that OSDA-Me and OSDA-Pr mainly differed in the size of diammonium head groups. Obviously, the OSDA-Pr with tripropyl groups attaching to the terminal nitrogen atom possessed a larger molecular size than OSDA-Me. As the terminal ammonium head is located at the intersection of the MFI channels, reasonably, the quaternary ammonium cations of OSDA-Pr with a larger size would favor to be confined within the straight 10-MR channels. The organic species were then expected to be more stable against leaching. To remove the residual OSDA-Pr molecules physically absorbed loosely on the outface or within interlayer spaces, a mild acid treatment (HCl/EtOH) was carried out on as-synthesized LZSM-5-as sample once or twice, resulting in LZSM-5-AT and LZSM-5-AT2, respectively.

Figure 1 shows the XRD patterns of as-synthesized LZSM-5 together with its derivatives obtained by acid treatment. LZSM-5-as and LZSM-5-AT both possessed a typical multilamellar MFI structure, showing the diffractions caused by oriented growth of the crystals along the *b*-axis in the region of 2θ = 5–35° together with the mesophase diffraction in the low-angle region (2θ < 5°) as a result of the layered structure consisting of MFI sheets and surfactant micelles. The low-angle diffraction of LZSM-5-AT2 was still well resolved and stayed at the same 2θ position even after repeated acid treatment (Figure 1c). These results implied that the acid treatments did not change the multilamellar structure and the stacking sequence of nanosheets.

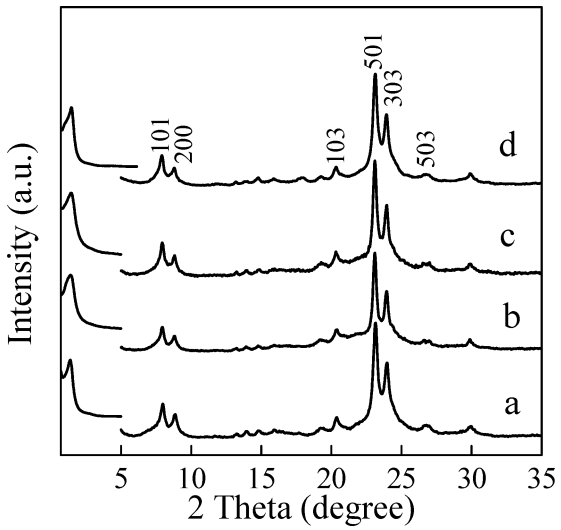

Figure 1. XRD patterns of (a) LZSM-5-as, (b) LZSM-5-AT, (c) LZSM-5-AT2, and (d) LZSM-5-AT–OH^-.

The SEM images show that LZSM-5-as exhibited a morphology of flower-like spheres (Figure 2a,b), which were composed of primary crystals with a palette morphology. The acid treatment did not change the crystal morphology (Figure 2c,d). The TEM investigation further confirmed that the LZSM-5-AT sample still maintained a multilamellar structure that contained 2.3 nm thick MFI nanosheets and 1.7 nm thick interlayer surfactant micelles (Figure 2e,f). Previous reports indicated the MFI nanosheets had only a single-unit-cell thickness of 2.0 nm *b*-axis based on HR-TEM images.[10] However, it was difficult to observe clearly the edge of thin crystalline sheets in TEM images, probably leading to an inaccuracy in thickness measurement. On the other hand, a simulation has been performed on the XRD pattern of layered MFI, which suggested the MFI nanosheets had 1.5 unit cells,[14] corresponding to 3 pentasil layers of 2.7 nm thickness along *b*-axis. Regardless of the slight difference in sheet thickness determined by different techniques, XRD and TEM measurements both verified that the multilamellar structure was well maintained even after acid washing. The acid treatment may remove selectively those physically absorbed OSDA-Pr

dx.doi.org/10.1021/cs500653p | ACS Catal. 2014, 4, 2959–2968

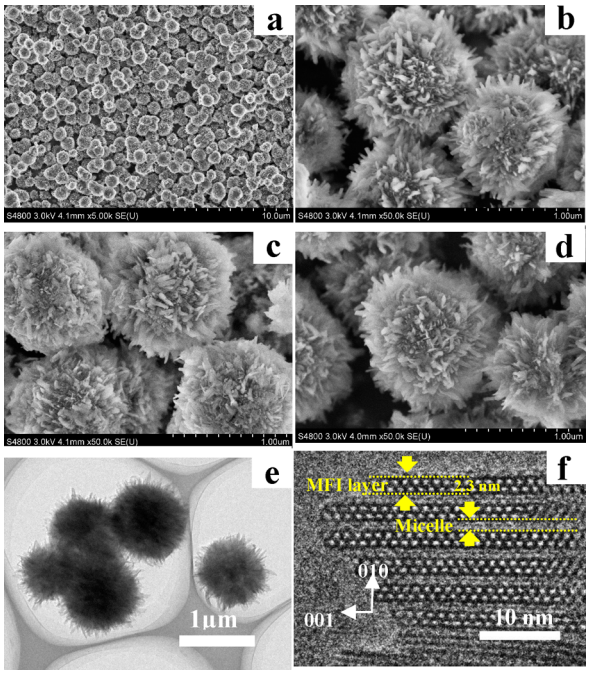

Figure 2. SEM images of (a, b) LZSM-5-as, (c) LZSM-5-AT, (d) LZSM-5-AT2, and TEM images of (e, f) LZSM-5-AT.

molecules but keep intact the residuals firmly blocked inside zeolite pores. The remaining long-chain alkyl groups of OSDA-Pr still pillared the MFI nanosheets. TG analysis indicated that the LZSM-5-as contained 25.6 wt % OSDA-Pr molecules (Figure S1a), whereas the weight percentage of OSDA-Pr in LZSM-5-AT decreased to 20.1 wt % (Figure S1b). Thus, the OSDA-Pr species removed by acid treatment accounted for 21.5% of total organic species, corresponding to those physically adsorbed on the crystal surface and loosely packed in interlayer spaces. After a further acid treatment, LZSM-5-AT2 still contained 19.8 wt % organic species (Figure S1c), almost the same as LZSM-5-AT. This implied that the residual OSDA-Pr molecules were highly stable against leaching.

LZSM-5-as possessed an extremely low nitrogen adsorption amount, mostly because the OSDA-Pr molecules jammed inside zeolite channels and interlayer spaces (Figure 3Aa). The isotherm of LZSM-5-as was still characteristic of type IV adsorption−desorption curves and gave a mesopore distribution at 4.2 nm by BJH calculation (Figure 3Ba), which is assigned to somewhat disorder stacking of nanosheets.[10] Above TEM observation indicated that the distance between adjacent MFI nanosheets was 1.7 nm (Figure 2f). The discrepancy given by these two techniques was probably due to the flexibility of this organic−inorganic hybrid structure in solvent ethanol upon ultrasonic treatment during HR-TEM measurement. LZSM-5-AT and LZSM-5-AT2 exhibited very comparable isotherms with much higher nitrogen adsorption amounts in comparison to LZSM-5-as (Figure 3Ab,Ac). The increased adsorption amount was because of a selective removal of physically absorbed OSDA-Pr species. Meanwhile, the mesopore distributions of LZSM-5-AT and LZSM-5-AT2 were still located at 4.2 nm (Figure 3Bb,Bc), but became more sharp than LZSM-5-as (Figure 3Ba), indicating that the lamellar structure was maintained and the stacking of nanosheets became more ordered after extracting removable OSDA-Pr. The surface area and pore volume increased greatly for LZSM-5-AT but changed slightly for LZSM-5-AT2 after second acid washing (Table 1). However, the calcined material, LZSM-5-AT-cal (Table 2, No. 5), showed a comparable specific surface area to that reported previously.[10a] The Si/Al molar ratio remained almost the same after acid washing, whereas the nitrogen content decreased from 0.75 mmol g^{-1} to 0.52 mmol g^{-1} after the first acid treatment and was kept at 0.51 mmol g^{-1} after the second treatment (Table 1). These results indicated that the tetrahedral Al atoms incorporated in the zeolite framework were stable upon acid washing, and only a part of OSDA-Pr molecules were removable.

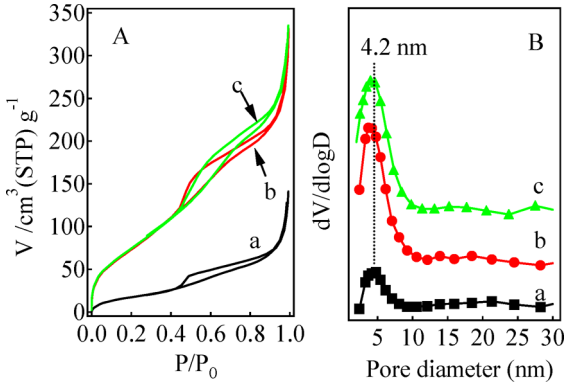

Figure 3. N_2 adsorption and desorption isotherms (A) and pore size distribution (B) of (a) LZSM-5-as, (b) LZSM-5-AT, and (c) LZSM-5-AT2.

Solid-state ^{13}C MAS NMR spectrum of LZSM-5-AT was almost the same with that of LZSM-5-as, further confirming that the remaining OSDA-Pr molecules were stable without decomposition during the acid washing process (Figure S2). ^{27}Al MAS NMR spectra of LZSM-5-as and LZSM-5-AT showed a signal resonance at 52 ppm (Figure 4), which is assigned to tetrahedrally coordinated Al in framework.[15] The presence of acid sites was confirmed by pyridine-adsorption IR technique. The band around 1546 cm^{-1} is due to the vibration of protonated pyridine and is characteristic of Brønsted acid sites.[16] As LZSM-5-AT−OH^- will be employed as the catalyst in the form of organic−inorganic hybrid material, the IR measurement was thus carried out not at an elevated temperature higher than 423 K. As shown in Figure 5, the adsorption and desorption of pyridine at 423 K developed a band at 1546 cm^{-1} for LZSM-5-AT−OH^-, indicating that it contained the framework Al-related Brønsted acid sites reachable by guest molecules. The straight 10-MR channels were filled with OSDA-Pr, and the material possessed a layered structure pillared by the long alkyl group of OSDA-Pr. Only those Al located on 10-MR pore entrance and on the surface of MFI nanosheets were accessible to pyridine molecules and contributed to the observed Brønsted acidity. For comparison, the adsorption and desorption of pyridine were conducted on the further calcined sample, LZSM-5-AT-cal. The bands at 1546 cm^{-1} due to pyridinium ion and the band at 1454 cm^{-1} due to coordinated pyridine were both observed (Figure 5Ac and 5Bc), confirming the presence of Brønsted and Lewis acid sites. On the other hand, after activating LZSM-5-AT with ammonia solution and further drying, the resultant LZSM-5-AT−OH^- sample possessed a weak basicity, as its suspension in water showed a pH value of 9 (Table 1). The layered structure was still preserved, as evidenced by the XRD pattern (Figure 1d), and the nitrogen content of LZSM-5-AT−OH^-

dx.doi.org/10.1021/cs500653p | ACS Catal. 2014, 4, 2959−2968

Table 1. Physicochemical Properties of Lamellar LZSM-5 Samples

sample	S_{BET}[a] ($m^2\ g^{-1}$)	V_{total}[b] ($cm^3\ g^{-1}$)	Si/Al[c]	N[d] (mmol g^{-1})	basicity (pH)[e]
LZSM-5-as	69	0.127	68	0.75	
LZSM-5-AT	293	0.366	70	0.52	9.0
LZSM-5-AT2	301	0.383	70	0.51	

[a]To avoid thermal decomposition of OSDA species, the samples were evacuated at 423 K for 5 h before N_2 adsorption at 77 K. [b]Calculated by P/P_0 = 0.95. [c]Given by ICP analysis. [d]Nitrogen content was determined by element analysis. [e]Suspension of catalyst (OH^- form, 10 mg) in distilled water (3 mL).

Table 2. Knoevenagel Condensation and One-Pot Tandem Deacetalization Knoevenagel Condensation on LZSM-5 and ZSM-5 Catalyst

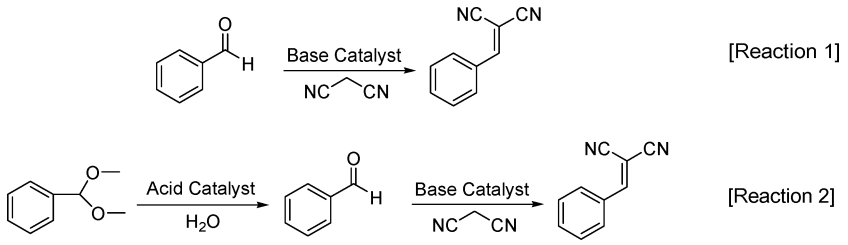

no.	cat.	Si/Al[a]	N content[b] (mmol g^{-1})	S_{BET}[c] ($cm^3\ g^{-1}$)	reaction 1[d]		reaction 2[e]		
					yield **BM** (mol %)	STY[f] (h^{-1})	yield **BA** (mol %)	yield **BM** (mol %)	STY[f] (h^{-1})
1	none				11.3		11.2	8.2	
2	$C_{18-6-3}(OH^-)_2$		3.58		80.6	124			
3	LZSM-5-as	68	0.75	69	95.6		23.6	2.1	
4	LZSM-5-AT−OH^-	70	0.52	293	92.6	142	7.3	91.2	23
5	LZSM-5-AT	70	0.52	289	86.4	133	10.6	86.1	22
6	LZSM-5-AT-cal	68		510	15.3		91.8	6.3	
7	LS-AT−OH^-	∞	0.50	272	88.2	141	0.9	5.3	1.4
8	ZSM-5-AT−OH^-	66	0.39	174	32.1		22.4	8.3	
9	ZSM-5-AT-cal	65		453	16.3		84.6	2.1	

[a]Obtained by ICP analysis. [b]By chemical element analysis. [c]Specific surface area measured by N_2 adsorption at 77 K and calculated by BET plot. [d]Reaction conditions: cat., 50 mg for heterogeneous catalyst, 0.0065 mmol for $C_{18-6-3}(OH^-)_2$; benzaldehyde, 2 mmol; malononitrile, 2 mmol; toluene, 3.6 g; temp., 353 K; time, 1 h. **BM**: benzylidene malononitrile. [e]Reaction conditions: cat., 50 mg; benzaldehyde dimethylacetal, 5 mmol; malononitrile, 5 mmol; acetonitrile, 2 mL; H_2O, 20 μg; temp., 353 K; time, 15 h. **BA**: benzaldehyde, **BM**: benzylidene malononitrile. [f]Site-time-yield (STY), moles of product per mol of N active sites per hour.

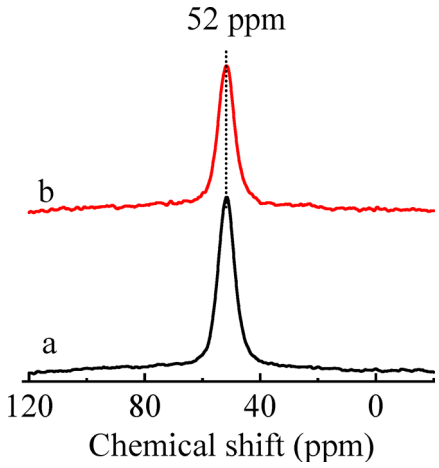

Figure 4. ^{27}Al MAS NMR spectra of (a) LZSM-5-as and (b) LZSM-5-AT.

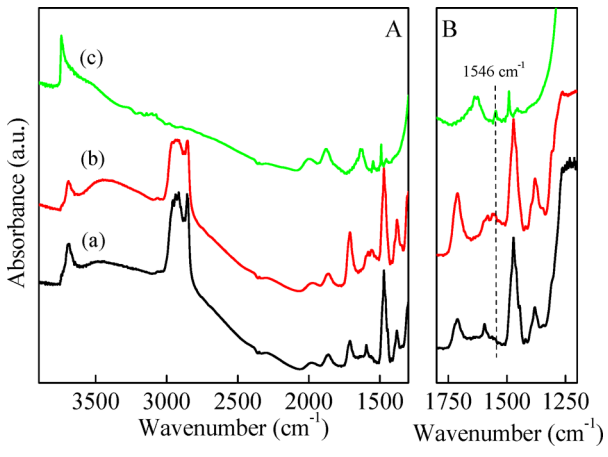

Figure 5. FT-IR spectra of LZSM-5-AT−OH^- after (a) degassing at 423 K for 2 h, (b) then further pyridine adsorption and desorption at 373 K for 2 h, and (c) the calcined LZSM-5-AT-cal after degassing at 723 K, further pyridine adsorption at room temperature and desorption at 723 K.

was identical to that of LZSM-5-AT (Table 2, Nos. 3 and 4), indicating the ion-exchange process showed no negative influence on the structure and chemical composition of LZSM-5-AT.

3.2. Catalytic Properties of LZSM-5-AT−OH^-. Aluminosilicates with OSDA molecules occluded in the channels can

dx.doi.org/10.1021/cs500653p | ACS Catal. 2014, 4, 2959−2968

be considered as solid acid−base materials. Isomorphous substitution of Al^{3+} ions in framework makes the lattice of crystalline zeolites negatively charged. The guest cations (e.g., protons, exchangeable metal cations or ammonium cations) are required to balance these negative charges. The protons bonded to negatively charged lattice oxygen atoms through ionic bonding form the hydroxyl groups of Brønsted acidity.[17] It has been also reported that the OSDAs in as-synthesized zeolite endow the negatively charged lattice oxygen atoms with Lewis basicity, which was assisted with quarternary ammonium cation.[7,18] On the other hand, the MFI nanosheet thickness was demonstrated to be 1.5 unit cells along *b*-axis.[14] According to the computational estimation on optimized molecular structure, the distance between two nitrogen atoms in OSDA-Pr is 0.89 nm. Therefore, when the terminal ammonium group was located at the intersection of straight and sinusoidal 10-MR channels, the other one was exposed outside the nanosheets, at least partially. An anion is needed to balance the positive charge of exposed ammonium cation. Thus, it is deduced that there were two types of base sites in LZSM-5-AT−OH^-. The SiO^- moieties near the exposed ammonium cations formed the Lewis base site, whereas the counteranion OH^- of exposed ammonium headgroup formed the Brønsted base site. On the other hand, after acid washing and ion-exchange with ammonia solution, the bridging hydroxyl groups related to the framework Al in LZSM-5-AT−OH^- contributed to Brønsted acidity. The quaternary ammonium hydroxide grafted on mesoporous MCM-41 silica was once reported to become a strong Brønsted base catalyst that could be an alternative to soluble bases in reactions such as Knoevenagel condensations, Michael additions, and aldol condensations.[19] In this sense, LZSM-5-AT−OH^- is considered to serve as a bifunctional catalyst containing accessible acid and base sites to guest molecules.

We first investigated the catalytic activity of LZSM-5-AT−OH^- in the Knoevenagel condensation of benzaldehyde (BA) with malononitrile to produce benzylidene malononitrile (BM), a simple reaction for testing the effectiveness of heterogeneous base catalysts.[19,20] The reactions were carried out in toluene at 353 K for 1 h (Table 2). BM was the predominant product with a selectivity higher than 99% in all cases. First, the amount of catalyst used was optimized. The BM product yield increased with increasing amount of LZSM-5-AT−OH^-, although it was almost leveled off (92.6−93.8%) at 50−70 mg of catalyst loading (Table S2). The condensation of benzaldehyde with malononitrile took place even in the absence of any catalyst, but giving a low BM yield of 11.3% (Table 2, No. 1). The BM yield was highly enhanced on LZSM-5-as and LZSM-5-AT−OH^-, reaching 95.6% and 92.6%, respectively (Table 2, Nos. 3, 4). These two catalysts both contained the OSDA-Pr species but were different in content and stability, as shown above. To confirm whether the reactions proceeded in a heterogeneous or a homogeneous way, we have carried out control experiments by hot filtration. After the reaction was carried out for 5 min, the catalyst powders were removed by filtration, and the reaction was continued at 353 K for another 55 min by stirring the liquid-phase mixture. As shown in Figure S3, the yields of BM achieved at 5 min were 48.9% and 26.5% on LZSM-5-as and LZSM-5-AT−OH^-, respectively. After removing the LZSM-5-AT−OH^- catalyst, the BM yield increased slightly, probably because of the contribution of the noncatalytic reaction. However, the BM yield was improved more remarkably after removing LZSM-5-as. These results verified that the reaction took place predominately in heterogeneous way on LZSM-5-AT−OH^- without leaching of organic species and at least partially homogeneously on LZSM-5-as. As reported previously,[7] the OSDA species locked in firmly in the as-synthesized zeolite were easily leached out of the solid into reaction mixture. Besides, the BM yield reached 80.6%, when an equal amount of $OSDA(OH^-)_2$ was used as homogeneous catalyst. In terms of turnover frequency (STY, moles of product per mole of N active sites per hour), LZSM-5-AT−OH^- showed a slightly higher catalytic activity (STY = 142 h^{-1}) than homogeneous catalyst (STY = 124 h^{-1}). The reason is that LZSM-5-AT−OH^- possessed both Brønsted and Lewis base sites, whereas the homogeneous catalyst had only a Brønsted site.

On the other hand, the acid treated sample LZSM-5-AT was also active to the condensation but showed a lower BM yield (86.4%) than LZSM-5-AT−OH^- (Table 2, No. 5). Although they contained the same content of N active sites, the counteranions of the exposed OSDA-Pr ammonium groups were Br^- or Cl^- ions in LZSM-5-AT without ammonia activation. Then, the negatively charged lattice oxygen-related Lewis base sites are presumed to be available to Knoevenagel condensation. The calcined sample, LZSM-5-AT-cal, did not convert benzaldehyde efficiently under identical conditions (Table 2, No. 6), because both Brønsted and Lewis base sites disappeared after decomposition of OSDA-Pr. These results indicated that a high catalytic performance was observed only when the aluminosilicate and quaternary ammonium formed a composite.

A high BM yield (88.2%) was achieved on Al-free LS-AT−OH^- (Table 2, No. 7), but it was slightly lower than that of LZSM-5-AT−OH^-. For control experiment, the conventional bulk ZSM-5 catalyst, as-synthesized sample with TPA^+ as OSDA but with a 3-dimensional MFI structure, was also applied to the condensation. The TPA^+ cations located at the intersection of two 10-MR channels were stable against acid washing or extraction, but inaccessible to guest molecules. Thus, although containing a relatively high nitrogen content (0.39 mmol g^{-1}), ZSM-5-AT−OH^- showed a BM yield of only 32.1% (Table 2, No. 8), which was mainly contributed by the lattice oxygen-related Lewis base sites associated with the TPA^+ cations at pore entrance or external surface. After removing TPA^+ by calcination, ZSM-5-AT-cal became almost inactive for the reaction (Table 2, No. 9), further implying that the Lewis basicity was closely related to the coexistence of OSDAs.

To investigate the acidic−basic catalytic behavior, LZSM-5-AT−OH^- was further applied to tandem deacetalization−Knoevenagel condensation by comparing with other catalysts. This one-pot reaction involved acid-catalyzed hydrolysis of benzaldehyde dimethylacetal to benzaldehyde (BA) intermediate and subsequent base-catalyzed Knoevenagel condensation with malonontrile to benzylidene malononitrile (BM).[21] Trace amount of water (20 μg, corresponding to 1.1 μmol) was introduced to induce the acid hydrolysis in first step. The bifunctional reaction occurred out effectively when the catalyst loading was no less than 50 mg (Table S3). Among the catalysts investigated, LZSM-5-AT−OH^- showed the highest yield for the final product BM (91.2%) together with a low yield of benzaldehyde intermediate (7.3%) (Table 2, No. 4). Besides, LZSM-5-AT with only Lewis base sites exhibited similar catalytic behavior as LZSM-5-AT−OH^- but a lower BM yield (86.1%) (Table 2, No. 5). Thus, both LZSM-5-AT and LZSM-5-AT−OH^- were effective acid−base bifunctional catalysts for this tandem reaction. The catalytic activity of

dx.doi.org/10.1021/cs500653p | ACS Catal. 2014, 4, 2959−2968

LZSM-5-AT was improved by ammonia activation, indicating that there are two aspects contributing to the catalytic reaction in terms of base sites.

As we discussed before, the LZSM-5-AT−OH^- possessed both Brønsted and Lewis base sites, whereas the LZSM-5-AT only had Lewis base sites. The contribution of OSDA-Pr to the acid−base catalytic behavior was confirmed by the results obtained with the tandem reaction on further calcined sample. After burning off the organic species totally, LZSM-5-AT-cal was still capable of catalyzing the first step effectively, giving a high yield of intermediate benzaldehyde (91.8%) (Table 2, No. 6). However, the second step of condensation was retarded significantly, resulting in an extremely low BM yield (6.3%). Lacking acid sites in the framework, Al-free LS-AT−OH^- was not active for this tandem reaction (Table 2, No. 7). On the other hand, although ZSM-5-AT−OH^- contained both acid and base sites, it showed low yields of benzaldehyde intermediate and BM (22.4% and 8.3%, respectively) (Table 2, No. 8). This is simply because only a limited outer surface of ZSM-5-AT−OH^- was available to the reaction. After removing TPA^+ by calcination, ZSM-5-AT-cal showed a lower BM yield, but a higher benzaldehyde yield of 84.6% as the acid sites inside the pore became useful for benzaldehyde dimethylacetal hydrolysis (Table 2, No. 9). On the other hand, ethyl cyanoacetate and diethyl malonoate were also employed as methylenic substrates. As shown in Table S4, the final product yield decreased obviously when malononitrile was used as the reactant, which is probably because that the basicity of catalyst was relatively weak.

The reaction pathway was further investigated by tracing the product distribution change with the reaction time on the LZSM-5-AT−OH^- catalyst (Figure 6). Clearly, the reaction

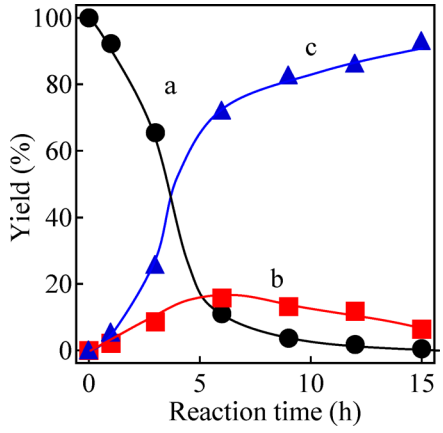

Figure 6. Results of the catalytic activity of the LZSM-5-AT−OH^- catalyst for the one-pot tandem deacetalization−Knoevenagel condensation reaction. Yields versus reaction time of (a) benzaldehyde dimethylacetal, (b) benzaldehyde, and (c) benzylidene malononitrile.

took place in two steps, that is, first hydrolysis of starting benzaldehyde dimethylacetal to benzaldehyde intermediate, and then Knoevenagel condensation with malononitrile to the final product BM, as graphically illustrated in Scheme 1. The product distributions exhibited typical behaviors of consecutive reactions, which occurred here with a synergetic cooperation of acid and base catalysis.

The reusability is an important feature of heterogeneous catalysts. We checked the durability of LZSM-5-AT−OH^- in the tandem deacetalization−Knoevenagel condensation. The

Scheme 1. Reaction Pathways of Acid−Base Bifunctional Tandem Reaction on LZSM-5-AT−OH^-

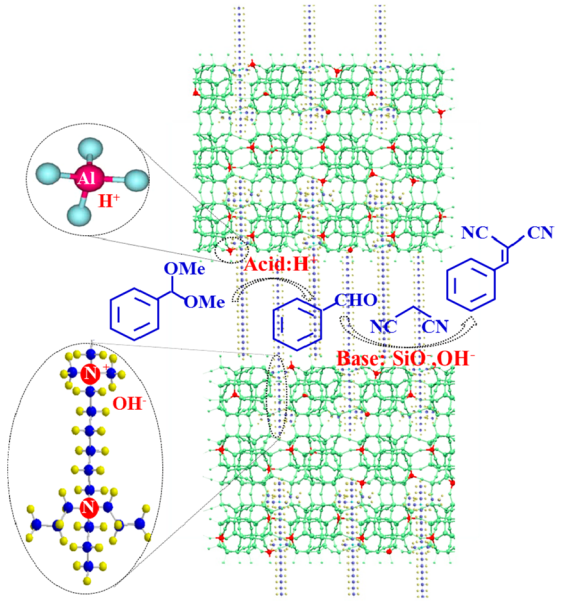

used catalyst was collected by filtration and washed with acetone. It was then subjected to the next run under the same reaction condition. As shown in Figure 7, there were no

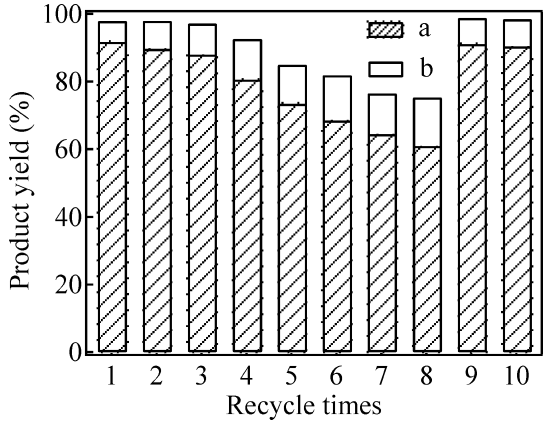

Figure 7. Reuse of LZSM-5-AT−OH^- in one-pot reaction of tandem deacetalization−Knoevenagel condensation. (a) Yield of benzylidene malononitrile, (b) yield of benzaldehyde.

significant decrease in BM and benzaldehyde yields after reuse for three times. The yields then began to decrease gradually with increasing the number of recycle and reuse, probably owing to the loss of Brønsted base sites. After the catalyst was used for eight times, it was regenerated by ion-exchange with ammonia solution to restore the Brønsted base sites. The regenerated catalyst showed almost totally restored activity in the ninth and tenth runs. These results confirmed that the counteranion OH^- was advantageous to the reaction. The TEM image taken on the LZSM-5-AT−OH^- catalyst used for 10 times showed well-preserved multilamellar MFI structure (Figure S4), indicating it was stable in structure and active sites.

It is worth noting that it is critical to choose suitable Gemini-type surfactants to design such a kind of rigid bifunctional catalyst. The most representative OSDA molecule used to synthesized multilamellar MFI nanosheets is OSDA-Me, in

dx.doi.org/10.1021/cs500653p | ACS Catal. 2014, 4, 2959−2968

which the diammonium groups bear four methyl groups.[10a,b] Thus, OSDA-Me has a much smaller cross-sectional area than OSDA-Pr. Not fixed firmly inside the 10-MR channels, OSDA-Me tended to be removed by post-treatments. In fact, the layer stacking became disordered, and the multilamellar structure was partially collapsed after repeated acid extraction (Figure S5). The TG analysis indicated that the weight percentage of OSDA-Me decreased from 36.8% to 31.1% after first acid treatment, and further to 20.5% after second treatment (Figure S6). N_2 adsorption indicated that the specific surface area and pore volume increased by repeated acid treatment (Table S1). These results implied that that the OSDA-Me species were removed gradually from LZSM-5-Me by repeated acid treatment. In this sense, LZSM-5-Pr exhibited a totally different character, as the two bulky propyl groups played an important role in immobilizing the OSDA-Pr species. Thus, LZSM-5-Me with OSDA-Me loosely inside channels cannot be used as a stable and reusable heterogeneous catalyst.

3.3. Catalytic Performances of Pd/LS-AT−OH⁻. Taking full advantage of the OSDA-related base catalytic behavior of layered MFI zeolites, it is highly desirable to develop a promising catalyst useful to tandem reaction involving a redox step. The active sites could originate from the precise metal nanoparticles (NPs), because it was demonstrated that the metal NPs supported on the materials with basic property were efficient to aerobic oxidation under mild and soluble-base-free conditions.[22] Herein, we supported Pd NPs on multilamellar MFI silicalite containing OSDA-Pr, and applied the resultant Pd/LS-AT−OH⁻ catalyst to one-pot tandem synthesis of benzylidene malononitrile from benzyl alcohol under soluble-base-free conditions. Before supporting Pd NPs, the as-made LS sample was subjected a mild acid washing and ion-exchange with ammonia solution before it was used as a catalyst in this one-pot reaction.

The XRD pattern of Pd/LS-AT−OH⁻ indicated that introduction of Pd NPs did not change the lamellar structure of the support, showing the ordered stacking of multilamellar MFI nanosheets in the low and wide angle (Figure 8). TEM observation revealed that highly dispersed Pd NPs with diameter of about 5 nm were successfully loaded on multilamellar MFI silicalite nanosheets in Pd/LS-AT−OH⁻ (Figure 9). Both the results of XRD and TEM have confirmed that the process of loading Pd NPs does not influence the structure order of support. The amount of Pd supported on LS-AT−OH⁻ was 0.26 wt %, and the X-ray photoelectron spectrum (XPS) of Pd/LS-1-AT−OH⁻ showed the Pd $3d_{5/2}$ and Pd $3d_{3/2}$ peaks at electron binding energies of 335.1 and 340.4 eV, respectively, indicating that the Pd species existed in a metallic state (Figure S7).

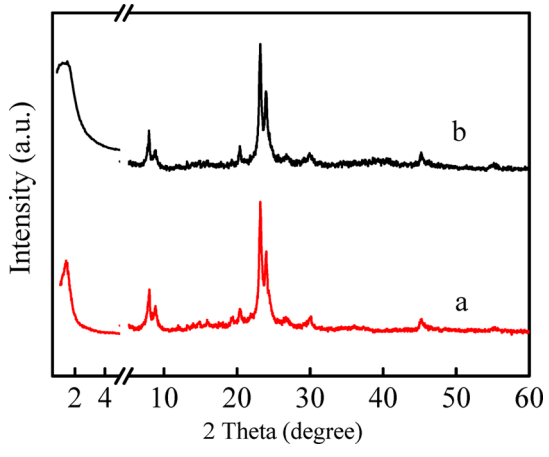

Figure 8. XRD patterns of (a) LS-AT and (b) Pd/LS-AT−OH⁻.

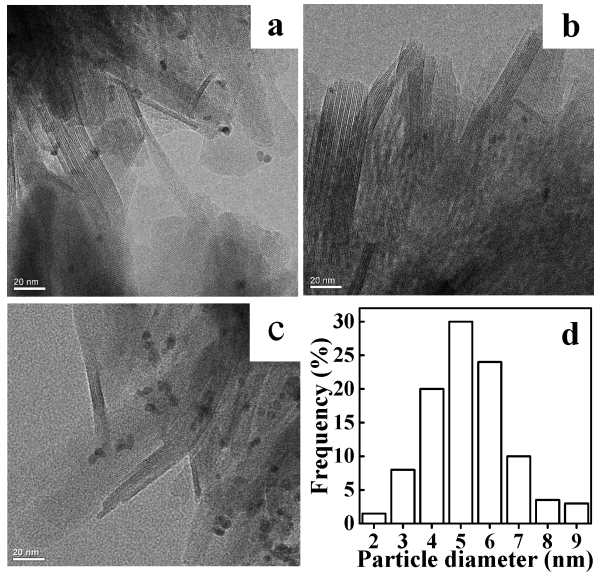

Figure 9. TEM images of Pd/LS-AT-1(a, b, c) and particle size distribution (d).

The catalytic activity of Pd/LS-AT−OH⁻ in the one-pot tandem synthesis of BM from benzyl alcohol was studied in toluene under oxygen atmosphere. The results are listed in Table 3. The one-pot synthesis of benzylidene malononitrile was realized through the oxidation of benzyl alcohol followed by Knoevenagel condensation with malononitrile. Benzaldehyde was produced as an intermediate and BM was the objective product in all cases. The LS-AT−OH⁻ support did not convert benzyl alcohol (Table 3, No. 1). On the other hand, Pd/S-1-as with 3D MFI structure and Pd/LS-AT-cal free of base sites showed low catalytic activity for this one-pot reaction (Table 3, Nos. 2, 3), although the maximum benzyl alcohol conversion and BM yield were achieved for the Pd/LS-AT−OH⁻ catalyst (Table 3, No. 4). These results indicated that Pd NPs supported on a basic material with an open structure were more suitable for this reaction. We also found that the Pd/LS-AT−OH⁻ catalyst was very efficient when a variety of primary alcohols were employed as the first-step reactants under similar reaction conditions (Table 3, Nos. 5−7). The reaction, however, was obviously retarded by using aromatic alcohol with an electron-withdrawing group, that is, 4-nitro benzyl alcohol (Table 3, No. 7). The condensation product yield (47.2%) was comparable to the alcohol conversion (48.6%), implying the oxidation was the rate-determining step.

On the other hand, when the condensation reactant malononitrile was substituted by ethyl cyanocaetate or diethyl malonate, the final product yield decreased obviously (Table 3, Nos. 8, 9). The benzyl alcohol conversion still reached 86.4−87.1%, and the yield of benzaldehyde intermediate was also as high as 83.0% in the case of diethyl malonate. This means the second condensation step was suppressed greatly, which made the whole one-pot synthesis inefficient for production. The Knoevenagel condensation is usually used to evaluate the catalyst basicity.[21] The condensation involving benzaldehyde

dx.doi.org/10.1021/cs500653p | ACS Catal. 2014, 4, 2959−2968

Table 3. Catalytic Performance of Different Pd-Based Catalysts in the Aerobic Oxidation−Knoevenagel Condensation[a]

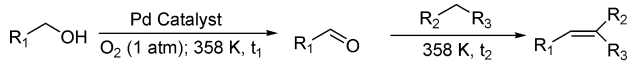

1 2 3

no.	cat.	R_1	R_2	R_3	time [t_1 + t_2] (h)	conv. [1][b] (mol %)	yield (mol %) 2	3
1	LS-AT−OH^-	C_6H_5	CN	CN	9 + 4	trace		
2	Pd/S-1-as	C_6H_5	CN	CN	9 + 2	13.2	0.3	12.9
3	Pd/LS-AT-cal	C_6H_5	CN	CN	9 + 2	8.8	0.5	8.3
4	Pd/LS-AT−OH^-	C_6H_5	CN	CN	9 + 2	89.6	0.5	88.3
5	Pd/LS-AT−OH^-	4-CH_3O−C_6H_5	CN	CN	9 + 2	92.1	2.7	89.2
6	Pd/LS-AT−OH^-	4-CH_3−C_6H_5	CN	CN	9 + 2	91.3	2.2	89.0
7	Pd/LS-AT−OH^-	4-NO_2−C_6H_5	CN	CN	12 + 2	48.6	1.4	47.2
8	Pd/LS-AT−OH^-	C_6H_5	CN	COOEt	9 + 6	87.1	48.4	38.7
9	Pd/LS-AT−OH^-	C_6H_5	COOEt	COOEt	9 + 14	86.4	83.0	3.2

[a]Reaction condition: see Experimental Section. [b]Conversion of alcohol.

and ethyl cyanocaetate or diethyl malonate is presumed to be catalyzed by strong base sites. Therefore, the catalytic results implied that the basicity of Pd/LS-AT−OH^- was relatively weak.

To track the reaction pathway more directly, the one-pot tandem synthesis of benzylidene malononitrile from benzyl alcohol was performed for different reaction time. As shown in Figure 10, the benzyl alcohol conversion and benzaldehyde

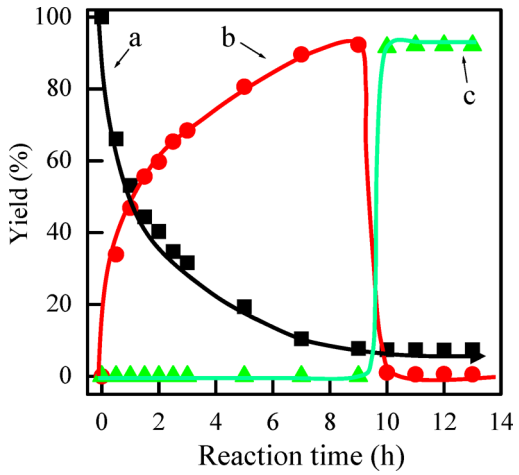

Figure 10. Results of the catalytic activity of Pd/LS-AT−OH^- for the one-pot tandem aerobic oxidation-Knoevenagel condensation reaction. Yields versus reaction time of (a) benzyl alcohol, (b) benzaldehyde, and (c) benzylidene malononitrile.

yield gradually increased to maximum values (>90%) within 9 h. After adding malononitrile into the reaction solution, the yield of intermediate benzaldehyde decreased rapidly to a low level, whereas the yield of benzyilidene malononitrile increased sharply and was leveled off at ca. 92%. This result verified that the one-pot synthesis occurred in a consecutive manner, and the oxidation of alcohol to aldehyde was the rate-controlling step.

4. CONCLUSIONS

The way to utilize organic-structure-directing agents in as-synthesized zeolite materials for catalytic purpose has been proposed. The multilamellar MFI aluminosilicate containing OSDA-Pr firmly immobilized inside channels proves to be an effective catalyst for acid−base tandem reaction. The quaternary organic ammonium salts not only can be act as structure-directing agents but also serve as catalytic active sites, resulting in bifunctional catalysts containing framework Al-related acid sites and OSDAs cations-related base sites. The organic−inorganic hybrid materials possess a rigid structure which is reusable and stable against leaching of organic species in catalytic reactions. To design that kind of stable bifunctional catalyst, it is critical to choose an OSDA with a large quaternary ammonium headgroup.

■ ASSOCIATED CONTENT

Supporting Information

Additional data and images as noted in the text. This material is available free of charge via the Internet at http://pubs.acs.org.

■ AUTHOR INFORMATION

Corresponding Author

*E-mail: pwu@chem.ecnu.edu.cn. Fax/Tel.: 86-21-62232292.

Notes

The authors declare no competing financial interest.

■ ACKNOWLEDGMENTS

We gratefully acknowledge the National Natural Science Foundation of China (21373089, U1162102, 21373004), Ph.D. Programs Foundation of Ministry of Education (2012007613000), the National Key Technology R&D Program (2012BAE05B02), and the Shanghai Leading Academic Discipline Project (B409).

■ REFERENCES

(1) (a) Čejka, J.; Corma, A.; Zones, S. In *Zeolites and Catalysis*; Wiley, Weinheim, 2010. (b) Corma, A. *J. Catal.* **2003**, *216*, 298−312. (c) Čejka, J.; Centi, G.; Perez-Pariente, J.; Roth, W. J. *Catal. Today* **2012**, *179*, 2−15. (d) Na, K.; Choi, M.; Ryoo, R. *Microporous Mesoporous Mater.* **2013**, *166*, 3−19.

(2) Wang, Z.; Yu, J.; Xu, R. *Chem. Soc. Rev.* **2012**, *41*, 1729−1741.

(3) (a) Burton, A. W.; Elomari, S.; Chan, I.; Pradhan, A.; Kibby, C. *J. Phys. Chem. B* **2005**, *109*, 20266−20275. (b) Elomari, S.; Burton, A. W.; Ong, K.; Pradhan, A. R.; Chan, I. Y. *Chem. Mater.* **2007**, *19*, 5485−5492. (c) Zones, S. I.; Burton, A. W.; Ong, K. International Patent WO/2007/079038, 2007.

(4) (a) Sun, J.; Bonneau, C.; Cantin, A.; Corma, A.; Diaz-Cabanas, M. J.; Moliner, M.; Zhang, D.; Li, M.; Zou, X. *Nature* **2009**, *458*, 1154−1157. (b) Jiang, J.; Jorda, J. L.; Diaz-Cabanas, M. J.; Yu, J.; Corma, A. *Angew. Chem., Int. Ed.* **2010**, *49*, 4986−4988. (c) Corma, A.; Diaz-Cabanas, M. J.; Jiang, J.; Afeworki, M.; Dorset, D. L.; Soled, S. L.; Strohmaier, K. G. *Proc. Natl. Acad. Sci. U.S.A.* **2010**, *107*, 13997−14002. (d) Jiang, J.; Yu, J.; Corma, A. *Angew. Chem., Int. Ed.* **2010**, *49*, 3120−3145.
(5) Gramm, F.; Baerlocher, C.; McCusker, L. B.; Warrender, S. J.; Wright, P. A.; Han, B.; Hong, S. B.; Liu, Z.; Ohsuna, T.; Terasaki, O. *Nature* **2006**, *444*, 79−81.
(6) (a) Lee, H.; Zones, S. I.; Davis, M. E. *Nature* **2003**, *425*, 385−388. (b) Lee, H.; Zones, S. I.; Davis, M. E. *Microporous Mesoporous Mater.* **2006**, *88*, 266−274.
(7) Kubota, Y.; Nishizaki, Y.; Ikeya, H.; Saeki, M.; Hida, T.; Kawazu, S.; Yoshida, M.; Fujii, H.; Sugi, Y. *Microporous Mesoporous Mater.* **2004**, *70*, 135−149.
(8) (a) Jones, C. W.; Tsuji, K.; Davis, M. E. *Nature* **1998**, *393*, 52−54. (b) Takewaki, T.; Beck, L. W.; Davis, M. E. *J. Phys. Chem. B* **1999**, *103*, 2674−2679. (c) Takewaki, T.; Beck, L. B.; Davis, M. E. *Top. Catal* **1999**, *9*, 35−42. (d) Jones, C. W.; Tsuji, K.; Takewaki, T.; Beck, L. W.; Davis, M. E. *Microporous Mesoporous Mater.* **2001**, *48*, 57−64.
(9) (a) Zeidan, R. K.; Hwang, S.-J.; Davis, M. E. *Angew. Chem.* **2006**, *118*, 6480−6483. (b) Zeidan, R. K.; Davis, M. E. *J. Catal.* **2007**, *247*, 379−382. (c) Sugino, K.; Oya, N.; Yoshie, N.; Ogura, M. *J. Am. Chem. Soc.* **2011**, *133*, 20030−20032. (d) Wang, X.; Chan, J. C. C.; Tseng, Y.-H.; Cheng, S. *Microporous Mesoporous Mater.* **2006**, *95*, 57−65. (e) Wang, X.; Lin, K. S. K.; Chan, J. C. C.; Cheng, S. *Chem. Commun.* **2004**, 2762−2763.
(10) (a) Choi, M.; Na, K.; Kim, J.; Sakamoto, Y.; Terasaki, O.; Ryoo, R. *Nature* **2009**, *461*, 246−250. (b) Na, K.; Choi, M.; Park, W.; Sakamoto, Y.; Terasaki, O.; Ryoo, R. *J. Am. Chem. Soc.* **2010**, *132*, 4169−4177. (c) Park, W.; Yu, D.; Na, K.; Jelfs, K. E.; Slater, B.; Sakamoto, Y.; Ryoo, R. *Chem. Mater.* **2011**, *23*, 5131−5137.
(11) (a) Kim, K.; Ryoo, R.; Jang, H.-D.; Choi, M. *J. Catal.* **2012**, *288*, 115−123. (b) Seo, Y.; Cho, K.; Jung, Y.; Ryoo, R. *ACS Catal.* **2013**, *3*, 713−720. (c) Na, K.; Jo, C.; Kim, J.; Ahn, W. S.; Ryoo, R. *ACS Catal.* **2011**, *1*, 901−907. (d) Wang, J.; Xu, L.; Zhang, K.; Peng, H.; Wu, H.; Jiang, J.; Liu, Y.; Wu, P. *J. Catal.* **2012**, *288*, 16−23.
(12) Shen, Z. H.; Liu, J.; Xu, H.; Yue, Y.; Hua, W.; Shen, W. *Appl. Catal., A* **2009**, *356*, 148−153.
(13) Na, K.; Park, W.; Seo, Y.; Ryoo, R. *Chem. Mater.* **2011**, *23*, 1273−1279.
(14) Varoon, K.; Zhang, X.; Elyassi, B.; Brewer, D. D.; Gettel, M.; Kumar, S.; Lee, J. A.; Maheshwari, S.; Mittal, A.; Sung, C.-Y.; Cococcioni, M.; Francis, L. F.; McCormick, A. V.; Mkhoyan, K. A.; Tsapatsis, M. *Science* **2011**, *334*, 72−75.
(15) Moliner, M.; González, J.; Portilla, M. T.; Willhammar, T.; Rey, F.; Llopis, F. J.; Zou, X.; Corma, A. *J. Am. Chem. Soc.* **2011**, *133*, 9497−9505.
(16) (a) Kim, K.; Ryoo, R.; Jang, H.-D.; Choi, M. *J. Catal.* **2012**, *288*, 115−123. (b) Wang, Y.; Liu, Y.; Wang, L.; Wu, H.; Li, X.; He, M.; Wu, P. *J. Phys. Chem. C* **2009**, *113*, 18753−18760.
(17) Schoonheydt, R. A.; Geerlings, P.; Pidko, E. A.; Santen, R. A. V. *J. Mater. Chem.* **2012**, *22*, 18705−18717.
(18) (a) Martins, L.; Boldo, R. T.; Cardoso, D. *Microporous Mesoporous Mater.* **2007**, *98*, 166−173. (b) Almeida, K. A.; Landers, R.; Cardoso, D. *J. Catal.* **2012**, *294*, 151−160. (c) Almeida, K. A.; Cardoso, D. *Catal. Today* **2013**, *213*, 122−126.
(19) (a) Rodriguez, I.; Iborra, S.; Corma, A.; Rey, F.; Jordá, J. *Chem. Commum.* **1999**, 593−594. (b) Rodriguez, I.; Iborra, S.; Corma, A. *Appl. Catal., A* **2000**, *194−195*, 241−252.
(20) Brooks, A. C.; France, L.; Gayot, C.; Li, J. P. H.; Sault, R.; Stafford, A.; Wallis, J. D.; Stockenhuber, M. *J. Catal.* **2012**, *285*, 10−18.
(21) (a) Motokura, K.; Fujita, N.; Mori, K.; Mizugaki, T.; Ebitani, K.; Kaneda, K. *J. Am. Chem. Soc.* **2005**, *127*, 9674−9675. (b) Motokura, K.; Tada, M.; Iwasawa, Y. *J. Am. Chem. Soc.* **2009**, *131*, 7944−7945. (c) Corma, A.; Diaz, U.; Garcia, T.; Sastre, G.; Velty, A. *J. Am. Chem. Soc.* **2010**, *132*, 15011−15021.
(22) (a) Liu, P.; Li, C.; Hensen, E. J. M. *Chem.—Eur. J.* **2012**, *18*, 12122−12129. (b) Xu, J.; Liu, Y.; Wu, H.; Li, X.; He, M.; Wu, P. *Catal. Lett.* **2011**, *141*, 860−865.